08,05

Study of structural and magnetic properties of epitaxial ⁵⁷Fe-enriched thin-film nanostructures during thermal oxidation

© I.V. Blinov, M.A. Milyaev, Yu.V. Korkh, T.V. Kuznetsova, I.K. Maksimova, A.V. Stolbovsky, A.Yu. Germov, B.Yu. Goloborodsky, R.M. Falahutdinov, E.V. Osinnikov, D.I. Devyaterikov

M.N. Mikheev Institute of Metal Physics, Ural Branch, Russian Academy of Sciences, Yekaterinburg, Russia

E-mail: blinoviv@mail.ru Received May 14, 2025 Revised May 30, 2025 Accepted June 4, 2025

This work investigates the effects of thermomagnetic treatment on the structural and magnetic properties of epitaxial layered structures $MgO(100)^{57}Fe(50\,\text{nm})/Cr(2\,\text{nm})$. Using X-ray diffraction, Raman spectroscopy, atomic force microscopy, and Mössbauer spectroscopy, we analyzed structural changes during annealing in the temperature range of $200-300\,^{\circ}C$. The study reveals that at temperatures above $250\,^{\circ}C$, oxygen diffusion through the protective Cr layer leads to the formation of antiferromagnetic α -Fe₂O₃. An increase in coercivity up to 190 Oe at $280\,^{\circ}C$ is attributed to exchange coupling between Fe and α -Fe₂O₃. However, no shift in the magnetic hysteresis loop (exchange bias) is observed, which may result from low magnetic anisotropy of hematite (α -Fe₂O₃) and structural and chemical inhomogeneity at the interlayer boundaries.

Keywords: Hematite (α -Fe₂O₃), unidirectional anisotropy, thermomagnetic treatment, oxygen diffusion, exchange bias, epitaxial thin films, interface engineering, magnetic nanostructures.

DOI: 10.61011/PSS.2025.06.61694.120-25

1. Introduction

The interest in metal nanostructures is caused by their unique physical and chemical properties, which differ substantially from the characteristics of volume materials and open new opportunities for use in nanoelectronics and spintronics [1]. The modern methods of synthesis and processing make it possible to shape the structure of such systems in a controlled manner, creating magnetic nanostructures with the specified functional properties. The key role in the formation of macroscopic characteristics of metal magnetic nanostructures is played by the features in the structure of separate layers and layer-to-layer boundaries, including the effects of phase-to-phase interaction, mutual diffusion of components and structural ordering in the near-boundary areas [2]. Systems of ferromagnetic/antiferromagnetic (FM/AF) type are of special interest), where targeted change in the structural parameters of layers and interfaces makes it possible to effectively control the magnetic properties, in particular — to create unidirectional anisotropy. The effect of the exchange coupling between ferromagnetic and antiferromagnetic materials at the interface in lamellar film structures is of interest, since it causes exchange bias $H_{\rm ex}$, and increases coercive force $H_{\rm c}$ of the FM/AF system compared to a single FM [3,4]. The exchange bias effect is widely used to create the information recording and storage devices, magnetoresistive memory and magnetic sensors [5,6]. Hematite α -Fe₂O₃ is potentially attractive for use in the systems with exchange coupling due to its high Néel temperature $T_{\rm N}=680\,^{\circ}{\rm C}$, which is an imporant characteristic determining the effective operation

of the media with exchange bias [6]. Hematite films may be produced by methods of magnetron sputtering, epitaxy and by thermal oxidation of Fe [7–9]. In the last case the control of the phase composition of formed oxides becomes especially important, since apart from α -Fe₂O₃, other iron oxides may be formed (FeO, γ -Fe₂O₃, Fe₃O₄), as well as hydroxides, which substantially impact the magnetic characteristics of the system [2,10–15].

This paper is dedicated to the study of the properties of magnetic nanostructures of FM/AF type, containing hematite α -Fe₂O₃. The results are presented on the study of the change in the structural and magnetic properties of epitaxial laminar structures MgO(100)/⁵⁷Fe/Cr under thermal oxidation. Use of isotope ⁵⁷Fe makes it possible to apply the method of nuclear γ -resonance spectroscopy for detailed analysis of phase transformations in process of thermomagnetic processing.

2. Experiment

Specimens MgO/ 57 Fe(50 nm)/Cr(2 nm) were prepared by molecular-beam epitaxy (MBE) method on upgraded setup "Katun-S" at pressure $1-5\cdot 10^{-8}$ Pa on single-crystal substrates MgO (100). Fe and Cr were evaporated from 57 Fe with 97.0% enrichment and Cr with purity of \geq 99.99% from ZrO₂ crucibles at substrate temperature 180 °C. Speed of Fe and Cr deposition was 0.15 and 0.12 nm/min, accordingly.

The layer of chromium with thickness of 2 nm serves to protect the structure against oxidation on air, selection of

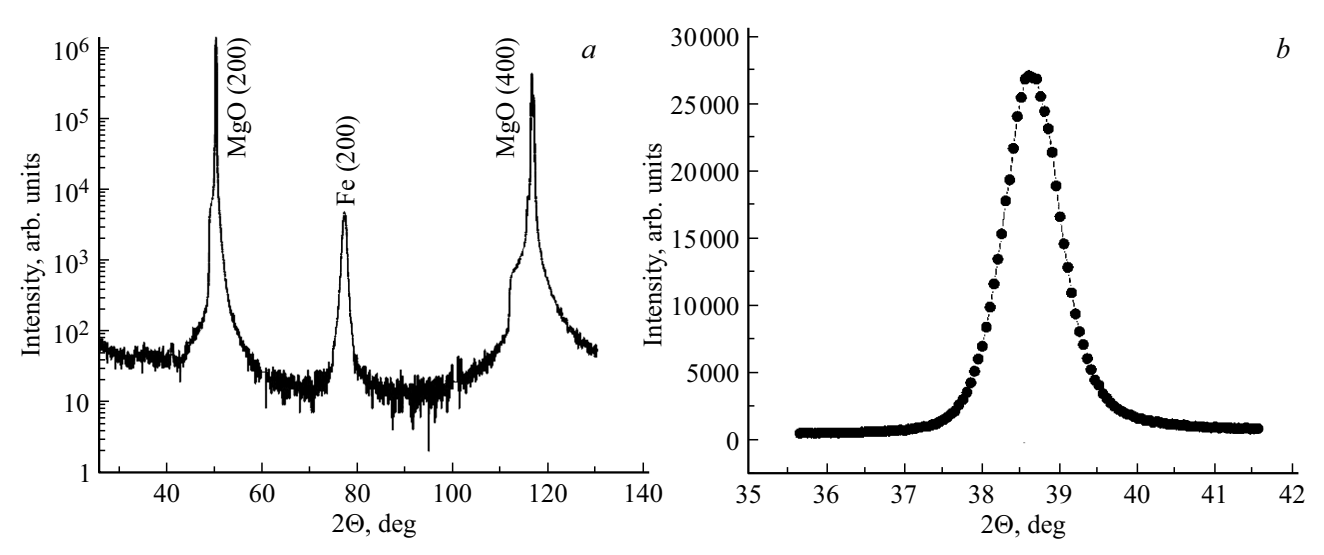


Figure 1. a — X-ray diffraction pattern of specimen MgO/ 57 Fe(50 nm)/Cr(2 nm); b — swing curve measured at diffraction line (200) Fe.

its thickness depends on the possibility of oxygen diffusion into Fe layer via Cr layer when annealed at atmospheric pressure. For film sputtering, Fe enriched with ⁵⁷Fe isotope was used, to be able to do Mössbauer spectroscopy.

Thermomagnetic treatment of the films was performed on an original design system in $2\,\mathrm{kOe}$ constant magnetic field applied in the specimen plane in the temperature range of $200-300\,^{\circ}\mathrm{C}$ during 60 min. at atmospheric pressure.

The structure was studied on X-ray diffractometer Philips PANalytical Empyrean in radiation CoK_{α} with geometry $\Theta-2\Theta$ of glazing incidence of the primary beam (glazing incidence X-ray diffraction, GIXRD). To obtain information on the texture perfection, the swing curves were measured.

The surface topography was studied with scanning probe microscope Solver Next. Raman scattering (RS) spectra of the specimens were obtained using the Confotec MR200 (SOL Instruments) confocal Raman microscope with 532 nm wavelength laser excitation. Mössbauer measurements were carried out using spectrometer CM-2201 at room temperature on ⁵⁷Fe nuclei in geometry of backscattering with conversion electron registration (conversion electron Mössbauer spectroscopy, CEMS) in a proportional flow-type counter. The source of γ -quanta was ⁵⁷Co in Cr. Direction of γ -quanta matched the normal line to the plane of the studied films. CEMS spectra were processed using specialized software for processing of Mössbauer spectra "Univem MS", which is based on model approach to spectra processing. The search for the optimal values of parameters in the model of Mössbauer spectra (δ -isomer shift, $Q_{
m S}$ quadrupole splitting and $H_{\rm hf}$ — effective magnetic field, including intensities of 2nd and 5th lines and partial inputs of subspectra) was carried out by the procedure included into the software to minimize χ^2 functionality, providing for the minimum deviation between the experimental spectrum and the considered models. The correspondence of the obtained models to the experimental spectra was confirmed by minimum values χ^2 , being within the limits of 1.0–1.2.

Hysteresis properties were studied using the ABM-1 computer-assisted vibration magnetometer in the auto mode at room temperature.

3. Results and discussion

Figure 1, a shows the X-ray diffraction pattern of the specimen after sputtering. The only structural peak is observed in the diffraction pattern at $2\Theta = 77.25\,^{\circ}$ from (200) Fe with the BCC lattice parameter Fe $a=0.287\,\mathrm{nm}$. Remaining structural peaks at $2\Theta=50.28$ and $116.38\,^{\circ}$ are related to a single-crystal substrate (200) MgO and (400) MgO accordingly. This indicates epitaxial growth of Fe film and availability of the crystalline texture $\langle 100 \rangle$ in Fe layer. The average crystallite size calculated using the Scherrer equation [16] is approximately 13 nm.

For quantitative assessment of the texture perfection evaluation, scattering angle of texture γ were measured. The corresponding swing curve is shown in Figure 1, b. Value γ is the average angle of deviation of orientation of some crystallites from the predominant orientation and is experimentally defined as full width at half maximum (FWHM) of swing curve (ω -scan) around the X-ray peak (200). To determine FWHM, swing curves were approximated with Gaussian function. Value γ is 0.8° , which indicates a highly perfect texture $\langle 100 \rangle$ formed in layer of Fe.

Peaks of light Raman scattering were also detected on the surface of the source specimen. Figure 2 provides the corresponding RS spectrum of film $MgO/^{57}Fe(50\,nm)/Cr(2\,nm)$.

The spectrum includes low-intensity peaks at frequencies 333 and $847\,\mathrm{cm}^{-1}$, corresponding to chromium oxide $\mathrm{Cr_2O_3}$ (low concentration of oxide, amorphous state). No iron oxide and oxyhydroxide phase vibrations were detected. It should be noted that epitaxial films Fe (100) have high corrosion resistance: thus, according to data of paper [17]

Table 1. Mössbauer spectra parameters (CEMS) of film $MgO(100)^{/57}Fe(50 \text{ nm})/Cr(2 \text{ nm})$. (G — widths of 1st and 6th lines of sextets, δ — isomer shift, Q_S — quadrupole splitting, H_{hf} — hyperfine magnetic field, S — area of the line of each sextet in % of the total area of the spectrum). Isomer shifts are given relative to α -Fe)

| G, mm/s | δ , mm/s | Q _S , mm/s | H_{hf} , kOe | S, % |
|-------------------|-------------------|-----------------------|-------------------------|------|
| 0.275 ± 0.009 | 0.005 ± 0.005 | -0.015 ± 0.009 | 330.5 ± 0.9 | 100 |

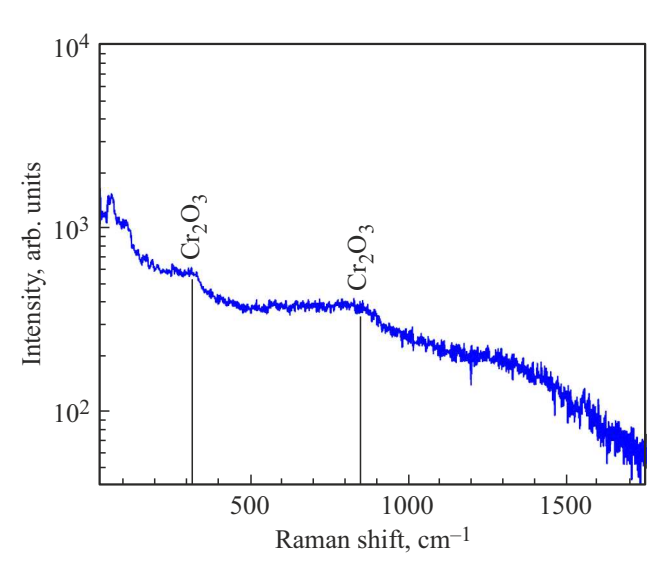


Figure 2. Raman light scattering spectrum $MgO/^{57}Fe(50 \text{ nm})/Cr(2 \text{ nm})$.

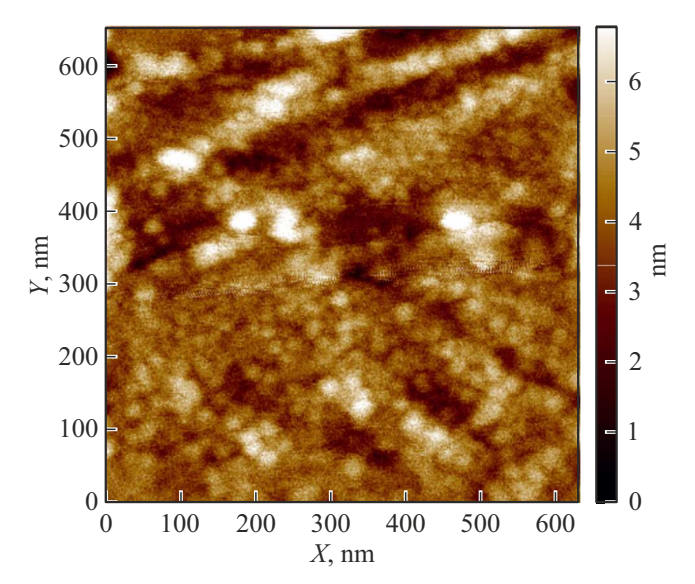


Figure 3. AFM-image of specimen MgO/Fe($50\,\mathrm{nm}$)/Cr($2\,\mathrm{nm}$) surface.

the thickness of oxide layer in film Fe not closed by a protective layer, when cured on air for a week does not exceed $0.5\,\mathrm{nm}$. It is natural to assume that formation of $\mathrm{Cr}_2\mathrm{O}_3$ is provided by the natural oxidation of layer Cr with thickness of $2\,\mathrm{nm}$, and the absence of diffraction

peaks of chromium oxide on the X-ray diffraction pattern is seemingly provided for by its X-ray amorphous state. Therefore, according to the data of X-ray diffraction and RS spectroscopy one may assume that thin layer of Cr_2O_3 prevents diffusion of oxygen into iron layer, formation of oxide and oxyhydroxide phases [18].

Figure 3 provides an AFM-image of MgO/Fe(50 nm)/Cr(2 nm) film surface after sputtering. The film surface is characterized by low mean square roughness $R_{\rm q}=0.20 \text{ nm}$. The specimen surface represents nanocrystallites with size of 10-15 nm. Such structure of the surface was also observed in papers [17,19] and is provided for by heteroepitaxial growth of film Fe [20].

The experimental Mössbauer spectrum of the specimen after sputtering is given in Figure 4. The points indicate the experimental values, the model spectrum is indicated with a solid line. CEMS parameters are presented in Table 1. The estimated spectrum is Zeeman sextet that belongs to phase α -Fe, and confirms the magnetic-ordered state of Fe layer. No compounds of oxides and oxyhydroxides of iron are found, which confirms the results obtained by the methods of X-ray diffraction and RS spectroscopy. The ratio of intensities of spectral lines is close to 1:4:3:3:4:1 and indicate the direction of the magnetic moment of the phase α -Fe along the plane of the film (perpendicularly to direction of γ -beams).

Figure 5, a shows magnetic hysteresis loops of the specimen measured at orientation of the magnetic field along the easy [100] Fe and difficult [110] Fe directions.

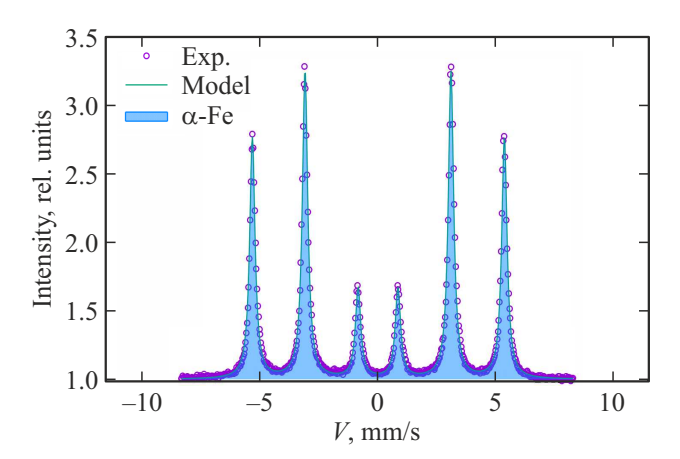


Figure 4. Mössbauer spectrum (CEMS) of film MgO(100)/ $^{57}Fe(50 \text{ nm})/Cr(2 \text{ nm})$.

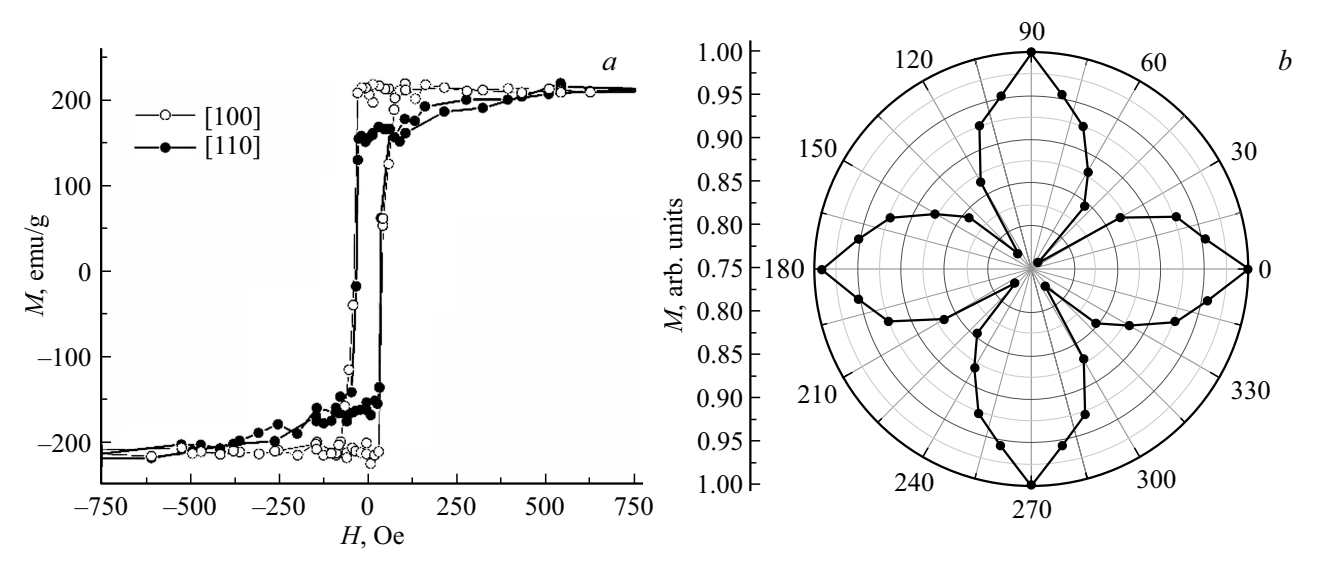


Figure 5. a — Magnetic hysteresis loops $MgO(100)/^{57}Fe(50 \text{ nm})/Cr(2 \text{ nm})$, measured along easy [100] and difficult [110] directions in the film plane; b — angular dependence of relative magnetization $MgO(100)/^{57}Fe(50 \text{ nm})/Cr(2 \text{ nm})$, measured as the specimen rotates in the magnetic field with intensity of 100 Oe.

From Figure 5 you can see that the hysteresis loop measured along [100] attains the saturation faster compared to the loop along [110]. Coercive force $H_{\rm c}$ [100] = 40 Oe is slightly higher than $H_{\rm c}$ [110] = 33 Oe, which indicates the presence of anisotropy in the film plane. Field of magnetic anisotropy ($H_{\rm a}$), defined as the crossing point of high-field areas of hysteresis loops measured along the easy and difficult axes of magnetization [21] is $H_{\rm a} = 500$ Oe. The produced values of anisotropy field and saturation magnetization $M_{\rm s} = 212$ emu/g are close to values $H_{\rm a}$ and $M_{\rm s}$ for massive Fe.

The availability of magnetic anisotropy in the specimen is confirmed by the data of angular dependence of magnetization as well. Figure 5, b shows a polar diagram of relative magnetization, measured in magnetic field $H=100\,\mathrm{Oe}$, lying in the film plane. The obtained data indicates that the plane of film Fe contains anisotropy of 4th order.

For formation of the oxide AF phase of hematite, as a result of exchange coupling, the source specimens were exposed to the procedure of annealing in the magnetic field with intensity of 2000 Oe at atmospheric pressure. Magnetic field in annealing and measurement was directed along [100] Fe.

Figure 6 shows magnetic hysteresis loops of specimens after thermomagnetic treatment at $T_{\rm a}=200,\ 250,\ 280$ and 300 °C with duration of 60 min. Ratio $M/M_{\rm s}^0$ is plotted along the vertical axis (M — magnetization of the specimen after annealing, $M_{\rm s}^0$ — magnetization of the same specimen before thermomagnetic treatment).

After annealing at $T_a = 200\,^{\circ}\mathrm{C}$ minor growth of H_c is observed from 40 to 50 Oe, and the ratio M/M_s^0 , which characterizes the reduction of the Fe volume fraction after annealing does not change. That is, such temperature effect is not sufficient for diffusion of oxygen into Fe

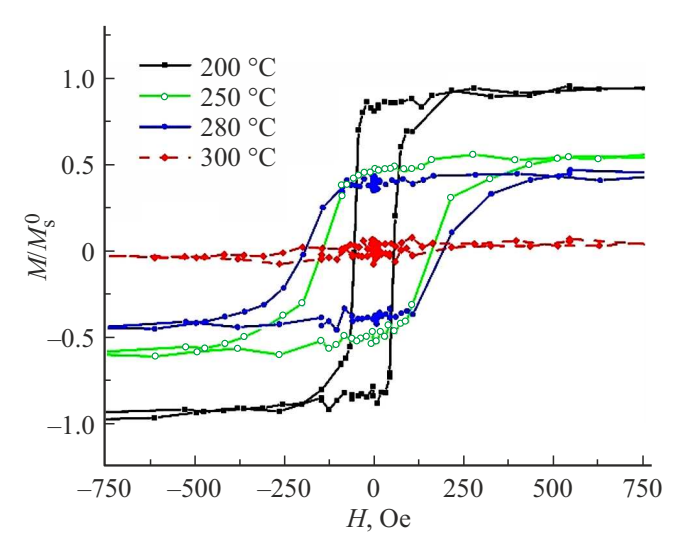


Figure 6. Magnetic hysteresis loops $MgO(100)^{57}Fe(50 \text{ nm})/Cr(2 \text{ nm})$ after annealing at temperatures 200, 250, 280, 300 °C. Annealing duration is — 60 min.

layer and formation of oxide phases, and layer Cr_2O_3 still acts as a diffusion barrier. As the annealing temperature rises to $T_a=250\,^{\circ}\mathrm{C}$, hysteresis properties change significantly: Hc increases to 150 Oe, and M/M_s^0 decreases to 0.55. At $T_a=280\,^{\circ}\mathrm{C}$ H_c achieves the maximum value of 190 Oe, and the FM fraction in Fe phase decreases to 0.41. After annealing at $T_a=300\,^{\circ}\mathrm{C}$ the ratio M/M_s^0 decreases practically to 0, which means absence of FM phase Fe in the film. It is natural to assume that in such thermal treatment mode the film structure consists fully of oxide phases. Recorded changes of hysteresis properties at $T_a=250$ and $280\,^{\circ}\mathrm{C}$ may be due to several reasons.

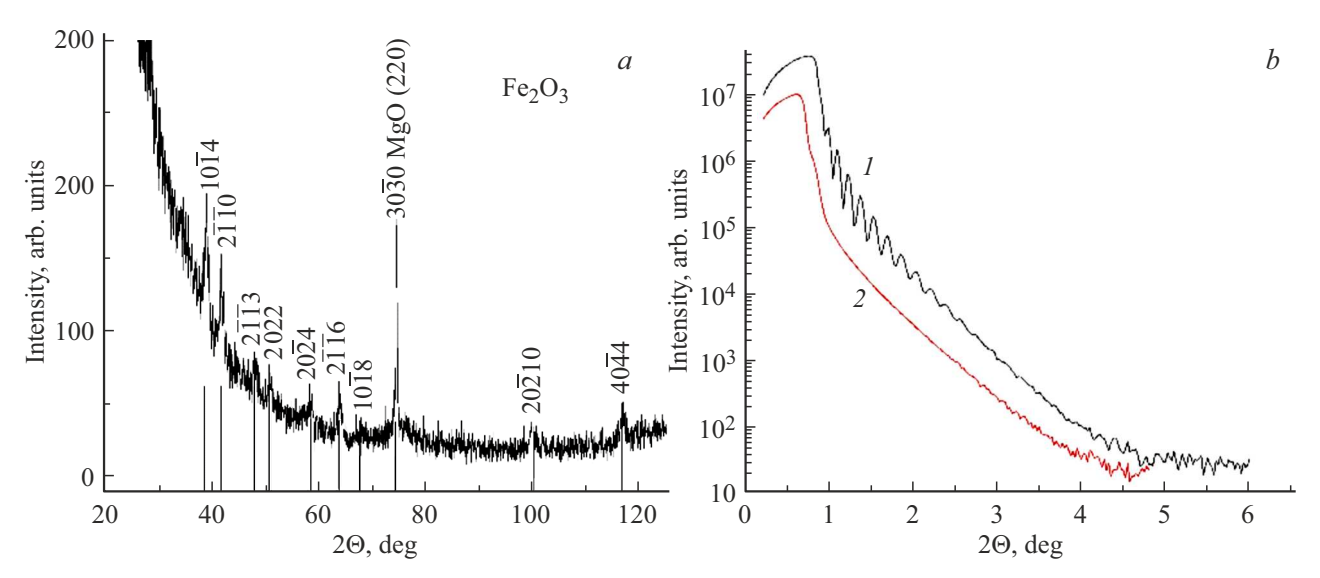


Figure 7. a — GIXRD diffraction pattern of MgO/ 57 Fe(50 nm)/Cr(2 nm) specimen after annealing at $T_a = 250$ °C-60 min; b — reflection curves of X-ray reflectometry for MgO/ 57 Fe(50 nm)/Cr(2 nm) specimen before (1) and after (2) annealing $T_a = 250$ °C (t = 60 min).

Firstly, decrease of M/M_s^0 is obviously connected to the oxygen diffusion to Fe layer and decrease in Fe volume fraction. Oxygen penetration into Fe through layer Cr₂O₃ happens in the boundaries of crystallites of chromium oxide nanocrystalline layer. Volume diffusion in this case is This conclusion may be made on the basis excluded. of the information on diffusion constants [22]. Thus, the values of coefficients of volume (D_b) and grain-boundary (D_{gb}) diffusion of O₂ into Cr₂O₃ at temperature 250 °C are equal to $D_b = 1.82 \cdot 10^{-37}$ and $D_{gb} = 2.67 \cdot 10^{-22}$ m/s², accordingly. Depth of penetration (x) of oxygen as a result of diffusion may be assessed using the following equation: $x = 2\sqrt{Dt}$ (1), where t — annealing time. The estimated depth of penetration for the time of annealing $\sim 60\,\mathrm{min}$ in the case of volume diffusion will be $\approx 10^{-8}$ nm, and in case of grain-boundary diffusion ≈ 2 nm, which makes it possible to conclude that penetration of oxygen into Cr₂O₃ happens along the paths of superfast diffusion, such as boundaries of crystallites, and penetration of oxygen into Cr₂O₃ via volume diffusion mechanism is practically excluded.

At the same time fast volume diffusion of oxygen into iron is observed ($D_b = 8.17 \cdot 10^{-22} \, \text{m/s}^2$ at $250 \, ^{\circ}\text{C}$) [23], therefore the volume depth of oxygen penetration into α -Fe at annealing temperature $250 \, ^{\circ}\text{C}$ (at $t = 60 \, \text{min}$) is $\approx 4 \, \text{nm}$, therefore, penetration of oxygen into a layer of iron via volume diffusion mechanism is most probable, besides, diffusion is possible along the paths of accelerated diffusion, firstly in high-angle grain boundaries.

In its turn, considerable growth of H_c in layer Fe is a typical sig of its FM exchange coupling with the fixing antiferromagnetic layer [3,4,6]. We believe that high values H_c in annealed specimens are due to the presence of antiferromagnetic phase α -Fe₂O₃ in the films.

To confirm the presence of α -Fe₂O₃ in the phase specimen at $T_a = 250\,^{\circ}\text{C}$ the X-ray and Mössbauer spectroscopy methods were used, as well as RS spectroscopy.

Figure 7, a shows the X-ray diffraction pattern of the specimen after annealing, obtained in the geometry of glazing incidence of the primary beam (GIXRD), the incident angle was 1°. Use of this geometry makes it possible to obtain a more intense signal from the surface layer, having low-textured polycrystalline structure. Main diffraction peaks observed in Figure 7, a are related to the crystalline phase α -Fe₂O₃. A non-mirror reflex from substrate MgO (220) is also observed in the spectrum. Figure 7, b presents curves of reflection of X-ray reflectometry before and after annealing. The period of oscillations in the curve of reflection of the source specimen corresponds to the total thickness of the film at 55 nm (at nominal thickness at 52 nm). The expressed Kiessign oscillations indicate highly advanced interfaces with low roughness. The reflection curve of film reflectometry after $T_a = 250$ °C-60 min contains no oscillations, which seemingly means substantial deterioration of interlayer boundaries and increase in the interface roughness. At the same time the reduction in the critical angle is observed, which is the expected result of the near-surface Fe layer oxidation.

Figure 8 shows the spectrum of Raman light scattering of the specimen after annealing at $T_a = 250\,^{\circ}\text{C}$. The spectrum includes high intensity narrow phonon peaks at frequencies 216, 235, 284, 400, 491, 600, 652, 809, 1065 and $1303\,\text{cm}^{-1}$, corresponding to the spectrum of pure iron oxide $\alpha\text{-Fe}_2\text{O}_3$, with high degree of crystallinity [24]. The peak at frequency $652\,\text{cm}^{-1}$, (marked with a star), related to $\alpha\text{-Fe}_2\text{O}_3$ according to data of papers [25,26], also complies with the frequencies of RS peaks in FeO and Fe $_3\text{O}_4$ oxides. Appearance of this peak is probably due to the presence of the phase between Fe and $\alpha\text{-Fe}_2\text{O}_3$

| Table 2. Mössbauer spectra parameters (CEMS) of film $MgO(100)/57Fe(50 \text{ nm})/Cr(2 \text{ nm})$ after annealing at $T_a = 250 ^{\circ}\text{C}$. (G — widths |
|---|
| of 1st and 6th lines of sextets, δ — isomer shift, Q_S — quadrupole splitting, H_{hf} — hyperfine magnetic field, S — area of the line of each |
| sextet in % of the total area of the spectrum). Isomer shifts are given relative to α -Fe) |

| Spectrum components | G, mm/s | δ , mm/s | $Q_{ m S}$, mm/s | H _{hf} , kOe | S, % |
|---|-------------------|-------------------|--------------------|-----------------------|----------------|
| α-Fe | 0.240 ± 0.009 | 0.005 ± 0.005 | -0.025 ± 0.009 | 330.0 ± 0.9 | 43.5 ± 0.9 |
| α-Fe ₂ O ₃ | 0.290 ± 0.009 | 0.350 ± 0.005 | -0.160 ± 0.009 | 513.0 ± 0.9 | 45.3 ± 0.9 |
| (Interface) Fe ²⁺ in iron oxide | 0.605 ± 0.009 | 0.815 ± 0.005 | 0.480 ± 0.009 | 432.5 ± 0.9 | 11.2 ± 0.9 |

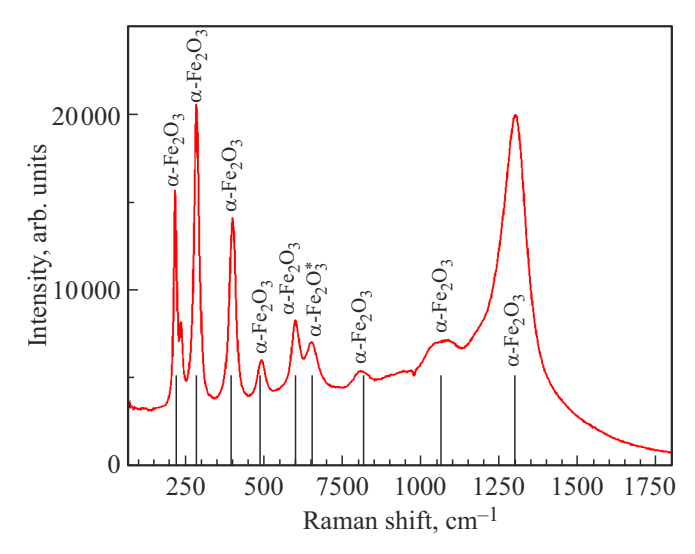


Figure 8. Raman light scattering spectrum MgO/Fe(50 nm)/ Cr(2 nm) after annealing at $T_a = 250 \,^{\circ}\text{C}$.

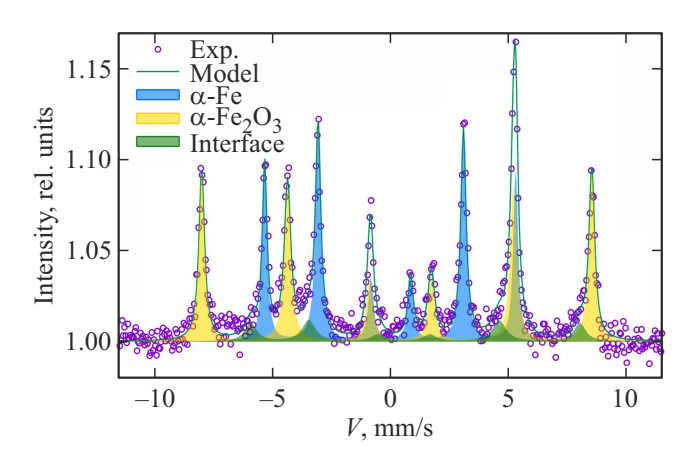


Figure 9. Mössbauer spectrum (CEMS) MgO/ 57 Fe(50 nm)/Cr(2 nm) after annealing at $T_a = 250$ °C (t = 60 min).

with intermediate valency of iron. No chromium oxide and oxyhydroxide phase vibrations were detected.

Figure 9 shows Mössbauer spectrum of the film after annealing at $T_a = 250$ °C. The points indicate the experimental values, the model spectrum is indicated with a solid line. CEMS spectrum parameters are presented in Table 2.

Good agreement of the experimental spectrum with the estimated one may be obtained, if the spectrum is presented in the form of three sextets, as shown in Figure 9. The Mössbauer spectrum, apart from the initial sextet from α -Fe (relative area of which in respect to the area of the entire spectrum is 43.5%), contains 2 additional sextets. Based on the modeling of Mössbauer spectra, one may state that the first sextet relates to antiferromagnetic iron oxide α -Fe₂O₃ (area — 45.3 %, $H_{\rm hf} = 513.0 \pm 0.9 \,\mathrm{Oe})$ [27,28]. Appearance of the second one (area — 11.2%, $H_{\rm hf} = 432.5 \pm 0.9 \, {\rm Oe}$), is probably due to atoms ⁵⁷Fe, located in the interface area between the oxide phase α -Fe₂O₃ and iron RCC. According to the literature data, it may be referred to Fe²⁺ in the mixed iron oxide Fe₃O₄ and Fe₂O₃, having lower values of hyperfine fields due to nanostate [29,30]. Its presence was expected, since the interface between these phases due to substantial difference in the lattice parameters is probably not fully coherent, and, accordingly, will have the structure that differs from the phases that form the interface [31].

Figure 10 shows AFM-image of film surface after annealing. After thermal treatment the specimen surface is structured, $R_{\rm q}$ is 5.0 nm. Ordered high columnar clusters α -Fe₂O₃ with base size of around 100 nm having cylindrical needle-shaped growths are formed on the surface. The data obtained are in qualitative agreement with the data of papers [32–34].

Therefore, the obtained results indicate the formation of magnetic-ordered phase $\alpha\text{-Fe}_2O_3$ in the specimen as a result of annealing.

It should also be noted that no displacement of the magnetic hysteresis loop in the entire studied interval of temperatures was recorded. Absence of displacement, probably, is due to low magnetic anisotropy α -Fe₂O₃. According to the data of paper [35], the crystallites having low magnetic anisotropy, do not have a stable state, and their magnetic switching occurs jointly with the FM layer, therefore causing growth H_c . Increase in anisotropy is possible by additional thermal treatment in magnetic layer [36]. Besides, the state of the interface area between two materials plays a key role in formation of exchange coupling [37,38]. Presence of the interface area according to the data of Mössbauer spectroscopy (11% of the spectrum area), with parameters different from Fe

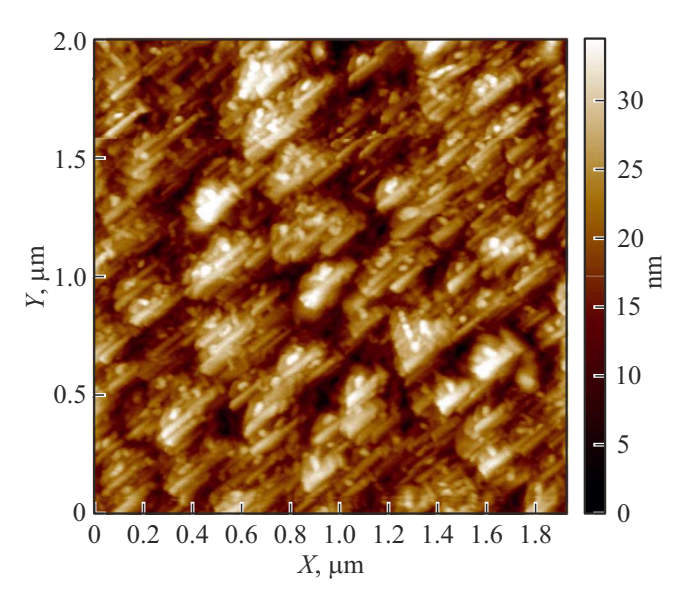


Figure 10. AFM-image of specimen MgO/ 57 Fe(50 nm)/Cr(2 nm) after $T_a = 250$ °C.

and α -Fe₂O₃, probably, indicates its structural and chemical heterogeneity, and possible presence of compounds that reduce the efficiency of the interlayer bond.

4. Conclusion

Methods of X-ray diffraction, spectroscopy, AFM-microscopy Mössbauer spectroscopy and properties of structural were used to study the MgO(100)/57Fe(50 nm)/epitaxial film structures Cr(2 nm) after thermomagnetic treatment in the interval of 200-300 °C. It was established that at annealing above 250 °C the AF phase of hematite α-Fe₂O₃ is formed in the films in the form of columnar clusters with the size of around 100 nm. Besides, oxygen penetrates mostly in the grain boundaries of chromium oxide Cr₂O₃ and further spreads to the iron layer using the mechanism of volume diffusion. The presence of the interface phase was recorded, which showed the imperfection of the interface. Changes of the magnetic properties under thermomagnetic treatment were studied. It was found that coercive force increases from 40 to 190 Oe as annealing temperature increases to 280 °C, and there is no displacement in the magnetic hysteresis loop.

Therefore, to create the materials with the controlled magnetic characteristics based on iron-hematite system, it is necessary to conduct additional thermomagnetic treatment and study the dynamics of the change in the state of interlayer boundaries in process of annealing.

Acknowledgments

X-ray, AFM studies were performed at Shared Research Facility "Test Center for Nanotechnology and Advanced Materials" Institute of Physics of Metals, Ural Branch, Russian Academy of Sciences.

Funding

The study was conducted with the financial support of the grant from the Russian Science Foundation and the Government of Sverdlovsk Region (project No. 24-22-20083).

Conflict of interest

The authors declare that they have no conflict of interest.

References

- [1] C. Zheng, K. Zhu, S.C. De Freitas. IEEE Transactions on Magnetics. 55, 4, 0800130 (2010).
 DOI: 10.1109/TMAG.2019.2896036
- [2] A.Y. Mohamed, W.G. Park, D.-Y. Cho. Magnetochemistry 6, 33 (2020). DOI: 10.3390/magnetochemistry6030033
- [3] T. Blachowicz, A. Ehrmann. Coatings 11, 122 (2021).DOI: 10.3390/coatings11020122
- [4] F. Radu, H. Zabel. In: Magnetic Heterostructures. Springer Tracts in Modern Physics, vol. 227. Springer-Verlag, Berlin, Heidelberg. (2008). P. 97.
- [5] L. Jogschies, D. Klaas, R. Kruppe. Sensors 15, 11, 28665 (2015). DOI: 10.3390/s151128665
- [6] R. Coehoorn. Novel Magnetoelectronic Materials and Devices: Handbook of Magnetic Materials. Elsevier, Amsterdam (2003)
- P. Li, C. Xia, Z. Zhu, Y. Wen, Q. Zhang, H.N. Alshareef,
 X.-X. Zhang. Adv. Funct. Mater. 26, 31, 5679 (2016).
 DOI: 10.1002/adfm.201504999
- [8] Y.X. Lu, J.S. Claydon, Y.B. Xu, S.M. Thompson, K. Wilson, G. van der Laan. Phys. Rev. B 70, 233304 (2004). DOI: 10.1103/PhysRevB.70.233304
- [9] S.S.A. Hassan, X. Yongbin, W. Jing, S.M. Thompson. IEEE Trans. Magn. 45, 10, 4357 (2009).DOI: 10.1109/TMAG.2009.2025600
- [10] V. Narayanaswamy, I.A. Al-Omari, A.S. Kamzin, C.V.V. Muralee Gopi, A. Khaleel, S. Alaabed, B. Issa, I.M. Obaidat. AIMS Mater. Sci. 9, 1, 71 (2022). DOI: 10.3934/matersci.2022005
- [11] A. Stierle, T. Mühge, H. Zabel. J. Mater. Res. 9, 884 (1994). DOI: 10.1557/JMR.1994.0884
- [12] M.J. Graham, R.J. Hussey. Oxid. Met. 15, 5/6, 407 (1981).DOI: 10.1007/BF00603533
- [13] R. Subbaraman, S.A. Deshmukh, S. K.R.S. Sankaranarayanan. J. Phys. Chem. C 117, 5195 (2013).
- [14] Yu.V. Baldokhin, Yu.D. Perfiliev, L.A. Kulikov, M.A. Burnazyan. Vestnik Moskovskogo Universiteta. Khimiya. **56**, *2*, 91 (2015). (in Russian).
- [15] A. Marczynska, J. Skoryna, M. Lewandowski, L. Smardz.
 Acta Phys. Pol., A 127, 2, 549 (2015).
 DOI: 10.12693/APhysPolA.127.549
- [16] B.D. Cullity. Elements of X-Ray Diffraction. Addison- 314 Wesley, Inc., London. (1978).

- [17] I. Flis-Kabulska, B. Handke, N. Spiridis, J. Haber, J. Korecki. Surf. Sci. 507-510, 865 (2002). DOI: 10.1016/S0039-6028(02)01364-X
- [18] Md.A. Mohiddon, K.L. Naidu, M.G. Krishna, G. Dalba, S.I. Ahmed, F. Rocca. J. Appl. Phys. 115, 044315 (2014). DOI: 10.1063/1.4863309
- [19] T. Ashraf, C. Gusenbauer, J. Stangl, G. Hesser, R. Koch.
 J. Phys.: Condens. Matter 27, 036001 (2015).
 DOI: 10.1088/0953-8984/27/3/036001
- [20] K. Thurmer, R. Koch, M. Weber, K.H. Rieder. Phys. Rev. Lett. 75, 9, 1767 (????). DOI: 10.1103/PhysRevLett.75.1767
- [21] K.-Y. Wang, M. Sawicki, K.W. Edmonds, R.P. Campion, S. Maat, C.T. Foxon, B.L. Gallagher, T. Dietl. Phys. Rev. Lett. 95, 217204 (2005). DOI: 10.1103/PhysRevLett.95.217204
- [22] S.C. Tsai, A.M. Huntz, C. Dolin. Mater. Sci. Eng. A 212, 6 (1996). DOI: 10.1016/0921-5093(96)10173-8
- [23] R. Barlow. P.J. Grundy. J. Mater. Sci. 4, 797 (1969). DOI: 10.1007/BF00551075
- [24] E. Rani, V.K. Gupta, F. Gyakwaa, M. Kharbach, H. Singh, T. Alatarvas, A. Martinelli, T. Fabritius, M. Huttula. Results Mater. 23, 100598 (2024). DOI: 10.1016/j.rinma.2024.100598
- [25] A. Koziol-Rachwal, N. Kwiatek, W. Skowronski, K. Grochot, J. Kanak, E. Madej, K. Freindl, J. Korecki, N. Spiridis. Phys. Rev. B 106, 104419 (2022). DOI: 10.1103/PhysRevB.106.104419
- [26] A.C. Sparavigna. Raman Spectroscopy of the Iron Oxides in the Form of Minerals, Particles and Nanoparticles. (2023) DOI: 10.26434/chemrxiv-2023-22kh4-v2
- [27] B.M. Gleeson, S.M.M. Hadavi, D.J. Young. Mater. High Temp. 17, 2, 311 (2000). DOI: 10.3184/096034000783640776
- [28] T. Fujii, M. Takano, R. Kakano, Y. Isozumi, Y. Bando. J. Magn. Magn. Mater. 135, 231 (1994).
 DOI: 10.1016/0304-8853(94)90351-4
- [29] A.G. Roca, J.F. Marco, M. del Puerto Morales, C.J. Serna. J. Phys. Chem. C 111, 50, 18577 (2007). DOI: 10.1021/jp075133m
- [30] G.M. da Costa, C. Blanco-Andujar, E. De Grave, Q.A. Pankhurst. J. Phys. Chem. B 118, 11738 (2014). DOI: 10.1021/jp5055765
- [31] E. Młyńczak, K. Freindl, N. Spiridis, J. Korecki. J. Appl. Phys. 113, 2, 024320 (2013). DOI: 10.1063/1.4775707
- [32] B. Tsedenbal, I. Hussain, M.S. Anwar, B.H. Koo. J. Nanosci. Nanotechnol. 18, 9, 6127 (2018). DOI:/10.1166/jnn.2018.15614
- [33] Q. Zhang, X. Lu, L. Chen, Y. Shi, T. Xu, M. Liu. Mater. Lett. 106, 447 (2013). DOI: 10.1016/j.matlet.2013.08.029
- [34] J.F. Mir, S. Rubab, M.A. Shah. Chem. Phys. Lett. **741**, 137088 (2020). DOI: 10.1016/j.cplett.2020.137088
- [35] K. O'Grady, L.E. Fernandez, G. Vallejo-Fernandez. J. Magn. Magn. Mater., 322, 883 (2010). DOI: 10.1016/j.jmmm.2009.12.011
- [36] A. Harres, J. Geshev. J. Phys.: Condens. Matter. **24**, *32*, 326004 (2012). DOI: 10.1088/0953-8984/24/32/326004
- [37] A.E. Berkowitz, S.K. Sinha, E.E. Fullerton, D.J. Smith. J. Appl. Phys. 117, 172607 (2015). DOI: 10.1063/1.4914340
- [38] E. Mlynczak, P. Luches, S. Valeri, J. Korecki. J. Appl. Phys. 113, 234315 (2013). DOI: 10.1063/1.4811528

Translated by M.Verenikina